AIAA Guidance, Navigation, and Control Conference and Exhibit
16 - 19 August 2004, Providence, Rhode Island

AIAA 2004-4900

A New Nonlinear Guidance Logic for Trajectory Tracking

Sanghyuk Park*, John Deyst†, and Jonathan P. How‡
Massachusetts Institute of Technology, Cambridge, MA, 02139, USA

A new nonlinear guidance logic, that has demonstrated superior performance in guiding unmanned air vehicles (UAVs) on curved trajectories, is presented. The logic approximates a proportional-derivative controller when following a straight line path, but the logic also contains an element of anticipatory control enabling tight tracking when following curved paths. The method uses inertial speed in the computation of commanded lateral acceleration and adds adaptive capability to the change of vehicle speed due to external disturbances, such as wind. Flight tests using two small UAVs showed that each aircraft was controlled to within 1.6 meters RMS when following circular paths. The logic was ultimately used for air rendezvous of the two aircraft, bringing them in close proximity to within 12 meters of separation, with 1.4 meters RMS relative position errors.

Nomenclature

V	Vehicle velocity
L_1	A line defined from vehicle position to a reference point on a desired trajectory
η	Angle created from V to the line L_1 (clockwise direction is positive)
$a_{s_{cmd}}$	Acceleration command sideways i.e. perpendicular to vehicle velocity direction
d	Cross-track error
R	Radius of circle or circular segment
$\mathcal{L}$	Lyapunov function

I. Introduction

Two approaches can be considered for the problem of trajectory tracking. One method separates the vehicle guidance and control problems into an outer guidance loop and an inner control loop. The inner loop controls the vehicle to follow acceleration commands which are generated by the outer loop. Simple strategies, based on geometric and kinematic properties, are typically used in the outer guidance loop. The alternative method uses an integrated approach wherein the inner and outer loops are designed simultaneously. In this case, a number of modern control design techniques can be applied, such as receding horizon [1], differential flatness [2, 3] and neural network based adaptive controls [4].

In most actual flight applications the separate inner and outer loop approach is more commonly taken because it is usually simpler and well-established design methods are available for inner loop vehicle control. Linear controllers are commonly used for the outer loop guidance of an aircraft. Typically, proportional and derivative (PD) controllers are used on the cross-track error, which is the lateral deviation from a desired flight path. If the desired trajectory path is similar to a straight line, then this simple strategy will provide reasonably good outer loop performance. However, when tasks require tight tracking of complex curved paths, linear feedback on the cross-track error may not provide satisfactory performance. The guidance logic presented in this paper contains an anticipatory control element which overcomes the inherent limitation of feedback control in following curved paths.

*Post-doctoral Associate, Laboratory for Information and Decision Systems, MIT, sanghyuk@mit.edu
†Professor of Aeronautics and Astronautics, MIT, deyst@mit.edu
‡Associate Professor of Aeronautics and Astronautics, MIT, jhow@mit.edu. Senior Member AIAA.

There are several terminal phase guidance laws for short-range tactical missiles that can be used to do trajectory following by using an imaginary point moving along the desired flight path as a pseudo target. Of these, *proportional navigation* generally provides the best performance, with less control effort, in constant-velocity intercepts, and it is widely accepted as the preferred method of guidance [5–7]. The trajectory following guidance logic presented in this paper was motivated by this proportional navigation method. An important element in the proportional navigation is the use of the change in the line-of-sight between a missile and a target. A similar feature is also found in the trajectory following guidance logic between a vehicle and a pseudo target on a desired path.An important difference between the two methods is that, unlike the proportional navigation, the speed of the pseudo target is not taken into account in the trajectory tracking guidance logic. A detailed discussion on the relationship of the trajectory following guidance logic to proportional navigation is provided in Section II-B.

Section II introduces the guidance logic and describes related properties. While the guidance logic developed here is simple and easy to apply, it is shown to have a number of benefits over linear approaches for curved paths. First, it contains proportional and derivative controls on cross-track error. Second, it has an element of anticipation for the upcoming local desired flight path. This property enables tight tracking on curved flight trajectories. Third, it uses instantaneous vehicle speed in the algorithm. This kinematic factor adds an adaptive feature with respect to changes in vehicle inertial speed caused by external disturbances such as wind.

The algorithm is easily implemented, and flight test results showing excellent tracking performance are given in Section III. The proposed guidance logic was implemented in two unmanned air vehicles (UAVs) in the Parent Child Unmanned Air Vehicle (PCUAV) Project [8, 9] at MIT, under the sponsorship of Draper Laboratory.

II. The New Guidance Logic

The guidance logic presented in this paper selects a reference point on the desired trajectory, and generates a lateral acceleration command using the reference point.

Selection of Reference Point – The reference point is on the desired path at a distance (L_1) forward of the vehicle, as shown in Figure 1.

Lateral Acceleration Command – The lateral acceleration command is determined by

$$a_{s_{cmd}} = 2\frac{V^2}{L_1}\sin\eta \tag{1}$$

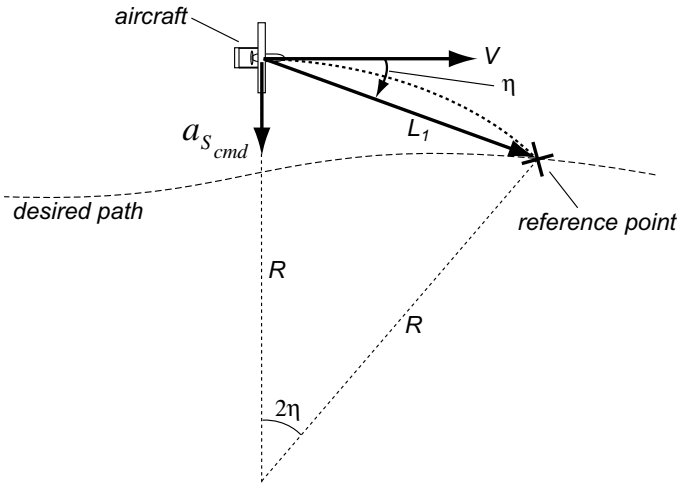

Figure 1. Diagram for Guidance Logic

Two properties of the guidance equation are significant.

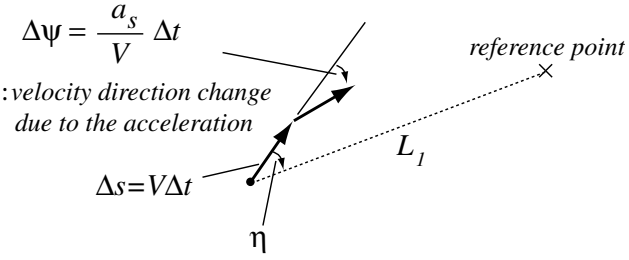

Figure 2. Discrete Representation : One Time Step

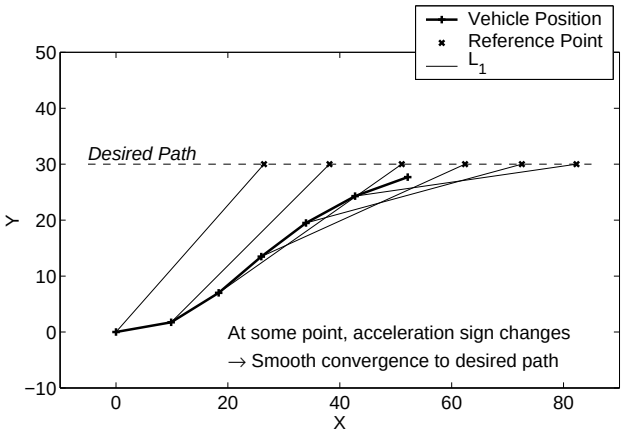

Figure 3. Discrete Representation : Step by Step (Δt=1, V=10, and L_1=40 are used in the simulation)

1. The direction of the acceleration depends on the sign of the angle between the L_1 line segment and the vehicle velocity vector. For example, if the selected reference point is to the right of the vehicle velocity vector, then the vehicle will be commanded to accelerate to the right, which is the case in Figure 1. In other words, the vehicle will tend to align its velocity direction with the direction of the L_1 line segment.

2. At each point in time a circular path can be defined by the position of the reference point, the vehicle position, and tangential to the vehicle velocity vector; as indicated by the dotted line in Figure 1. The acceleration command generated by Eq. (1) is equal to the centripetal acceleration required to follow this instantaneous circular segment. This is readily shown by noting that

$$L_1 = 2R\sin\eta \tag{2}$$

so

$$\text{centripetal acceleration} \;=\; \frac{V^2}{R} = 2\frac{V^2}{L_1}\sin\eta = a_{s_{cmd}}$$

Hence the guidance logic will produce a lateral acceleration that is appropriate to follow a circle of any radius R.

A. Characteristics of the Guidance Logic

This section describes a discrete time simulation that was performed to gain further insights about the performance of the nonlinear guidance law. First, consider Figure 2 showing the evolution of the guidance logic in one small time step increment. In this diagram, the reference point is to the right of the direction of the vehicle velocity. Therefore, at the next time step the velocity direction rotates clockwise due to the acceleration command.

With this one time step increment in mind, Figure 3 shows the trajectory of the vehicle over several time steps, where the vehicle initially starts from a location far away from the desired path, and eventually converges to the desired path. Given a certain length L_1 as shown in Figure 3, it can be inferred that

- The direction of L_1 makes a large angle with the desired path, when the vehicle is far away from the desired path.
- The direction of L_1 makes a small angle with the desired path, when the vehicle is close to the desired path.

Therefore, if the vehicle is far away from the desired path, then the guidance logic tends to rotate the vehicle so that its velocity direction approaches the desired path at a large angle. On the other hand, if the vehicle is close to the desired path, then the guidance logic rotates the vehicle so its velocity direction approaches the desired path at a small angle.

B. Relation to Proportional Navigation Guidance Laws

Consider the reference point as a target and the aircraft as a missile. Then, an interesting similarity is found in relation to proportional navigation missile guidance. The formula in Eq. (1) for the lateral acceleration command in the trajectory following guidance logic can be shown to be equivalent to the formula

$$a_{\perp LOS} = N' V_C \dot{\lambda}$$

for the acceleration command perpendicular to the line-of-sight in the proportional navigation with a navigation constant of N'=2, *under the assumption that the reference point is stationary* in the computation of the line-of-sight rate and the closing velocity. This equivalence can be shown using Figure 4. First, noticing that there is an angular difference between the vehicle lateral acceleration(a_s) and the acceleration($a_{\perp LOS}$) perpendicular to the LOS

$$a_{\perp LOS} = a_s \cos\eta$$

Using the acceleration command formula

$$a_s = 2\frac{V^2}{L_1}\sin\eta$$

leads to

$$a_{\perp LOS} = 2\frac{V^2}{L_1}\sin\eta\cdot\cos\eta = 2\left(V\cos\eta\right)\left(\frac{V}{L_1}\sin\eta\right)$$

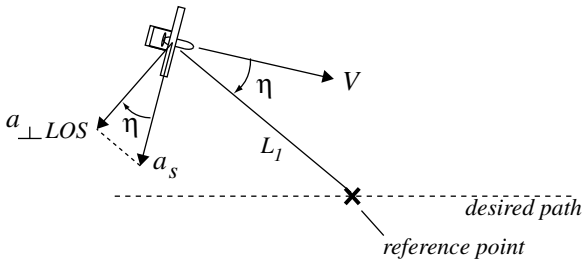

Figure 4. Relation with Proportional Navigation

where, assuming that the target point is stationary, the first bracket is the closing velocity (the relative velocity component in the direction of the LOS) and the second bracket is the LOS rate. Therefore, it can be shown that

$$a_{\perp LOS} = 2 \cdot V_C \cdot \dot{\lambda}$$

which is the form of the proportional navigation formula with the navigation constant equal to 2. However, the guidance logic (selection of reference point + acceleration command) cannot be explained only by the proportional navigation because the reference point is actually moving, and the closing speed between the reference point and the vehicle is always zero (with L_1 fixed).

C. Linear Analysis

In this section, linear analyses are performed for the following three cases:

- Case 1: following a straight line
- Case 2: following a non-straight line which is a perturbation from a straight line
- Case 3: following a circular path

and significant features are pointed out. An important design choice in the guidance logic is the distance L_1 between the vehicle and the reference point. This value can be chosen with the help of a linear system analysis.

Case 1: Following a Straight-line and Selection of L_1

Figure 5 defines the notation used in the linearization. L_1 is the distance from the vehicle to the reference point, d is the cross-track error, and V is a vehicle nominal speed. Assuming η is small in magnitude

$$\sin\eta \approx \eta = \eta_1 + \eta_2$$

and

$$\eta_1 \approx \frac{d}{L_1}, \qquad \eta_2 \approx \frac{\dot{d}}{V}$$

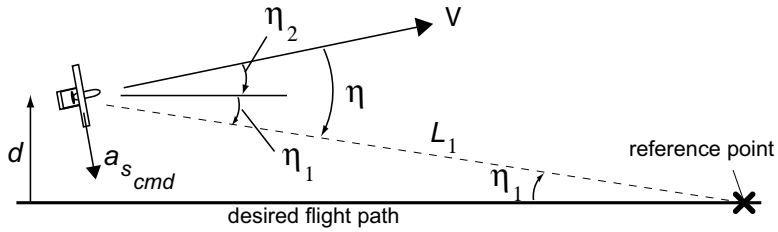

Figure 5. Linear Model for Straight-line Following Case

Combining the above with the guidance formula leads to

$$a_{s_{cmd}} = 2\frac{V^2}{L_1}\sin\eta \approx 2\frac{V}{L_1}\left(\dot{d} + \frac{V}{L_1}d\right) \tag{3}$$

Hence, linearization of the nonlinear guidance logic yields a PD (proportional and derivative) controller for the cross-track error. Also, the ratio of the vehicle speed V and the separation distance L_1 is an important factor in determining the gains of the proportional and derivative controllers. For instance, a small value for L_1 would lead to a high control gain and the ratio L_1/V determines the time constant of the PD controller.

The separation distance can be chosen by performing a stability analysis with the linear plant model and the derived linear controller. The plant model should include the vehicle dynamics with inner-loop bank angle controller (if bank angle is used to generate lateral acceleration for aircraft) and any sensor dynamics in the associated loop transmission function.

Furthermore, assuming no inner-loop dynamics and a small angle assumption on η_2, then $a_{s_{cmd}} \approx -\ddot{d}$ and Eq. (3) is equal to

$$\ddot{d} + 2\zeta\omega_n\dot{d} + \omega_n^2 d = 0 \quad \text{with} \;\; \zeta = 1/\sqrt{2},\; \omega_n = \sqrt{2}V/L_1 \tag{4}$$

Eq. (4) indicates that an approximate linear model, for the case of following a straight line, is a simple second order system that always has a damping ratio of 0.707 and its natural frequency is determined by the ratio of the vehicle speed and the length for the reference point selection.

Case 2: Following a Perturbed Non-Straight Line

The tracking capability on a curved path is demonstrated in this section by performing a linear analysis for a case with non-straight desired trajectory as shown in Figure 6. In this case the desired path is a perturbed

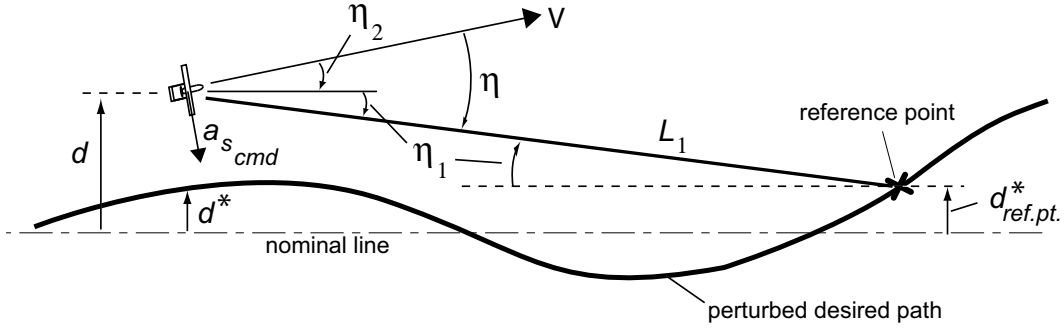

Figure 6. Linear Model for Non-straight Perturbed Line Following Case

curved line from a nominal straight line. In Figure 6, d is the lateral position of the current vehicle location and $d^{\star}_{ref.pt.}$ indicates the position of the reference point. Assuming the magnitude of the angles, η_1 and η_2 are small

$$\sin\eta \approx \eta = \eta_1 + \eta_2$$

Then, since

$$\eta_1 \approx \frac{d - d^\star_{ref.pt.}}{L_1}, \qquad \eta_2 \approx \frac{\dot{d}}{V}$$

and $a_{s_{cmd}} \approx -\ddot{d}$, the guidance law in Eq. (1) reduces to

$$\ddot{d} + \frac{2V}{L_1}\dot{d} + \frac{2V^2}{L_1^2}d = \frac{2V^2}{L_1^2}d^\star_{ref.pt.} \tag{5}$$

Taking the Laplace transforms of each term of Eq. (5) yields

$$\frac{d(s)}{d^\star_{ref.pt.}(s)} = \frac{\omega_n^2}{s^2 + 2\zeta\omega_n s + \omega_n^2} \quad \text{where } \zeta = 0.707,\ \omega_n = \frac{\sqrt{2}V}{L_1} \tag{6}$$

Eq. (6) represents a second order low-pass linear system with a unity steady state gain from the reference point input to the vehicle position. The damping ratio(ζ) is 0.707 and the undamped natural frequency(ω_n) is determined by $\sqrt{2}V/L_1$. The input of the transfer function in Eq. (6) is the lateral position of the reference point, not the position of the desired path at current vehicle location (*i.e.*, $d^\star_{ref.pt.}$ not $d^\star$). The use of a reference point in front enables phase recovery around the bandwidth frequency ω_n. For example, consider a sinusoidal trajectory command written as

$$d^\star = A\sin\left(\frac{2\pi x}{L_p}\right) \tag{7}$$

where A is a small path amplitude, L_p is a length-scale of the sinusoid, and x is distance along the path. Assuming $x \approx Vt$ then if $L_p = \sqrt{2}\pi L_1 \approx 4.4L_1$, the commanded trajectory expressed by Eq. (7) will excite the system at the bandwidth frequency (recall $\omega_n = \sqrt{2}V/L_1$). For a well-damped second order system as in Eq. (6) the phase *lag* at this frequency is 90 degrees. But this phase loss is from position input of the reference point $d^\star_{ref.pt.}$, not from $d^\star$, in Figure 6. Recalling that the reference point is at $L_1 = L_p/4.4$ (about a quarter of period) distance away, there will be about 90 degrees of phase *lead* in $d^\star_{ref.pt.}$ over $d^\star$. Therefore, these two effects will cancel each other, and the phase difference between the vehicle position and the desired path at current vehicle location (i.e. between d and $d^\star$) will be significantly reduced.

In general, considering the vehicle speed and the length for L_1, and assuming small angle for η there is a time difference of approximately L_1/V between $d^\star$ and $d^\star_{ref.pt.}$ i.e.

$$\frac{d^\star_{ref.pt}(s)}{d^\star(s)} \approx e^{\tau s}, \qquad \tau \approx L_1/V$$

Therefore, Eq. (6) can be written as

$$\frac{d(s)}{d^\star(s)} = \frac{\omega_n^2 e^{\tau s}}{s^2 + 2\zeta\omega_n s + \omega_n^2} \quad \text{where } \zeta = 0.707,\ \omega_n = \frac{\sqrt{2}V}{L_1},\ \tau \approx L_1/V \tag{8}$$

Bode diagrams for this system, as a function of L_1/L_p, are shown in Figure 7. The plot clearly shows the improvement in phase response near the system bandwidth (when $L_1/L_p \approx 1/4.4 = 0.23$) that results from the anticipation ($e^{\tau s}$). Furthermore, if L_p is the wavelength of the highest frequency content in the desired path, then L_1 must be chosen to be less than about $L_p/4.4$ if the vehicle is to accurately follow the desired path.

Case 3: Following a Circular Path

Figure 8 shows a diagram for a case of following a circular desired path. In this analysis η_1 and η_2 are assumed to be small, but η_3 is not necessarily small.

$$\eta_1 \approx 0, \quad \eta_2 \approx 0, \quad |\eta_3| \gg 0 \tag{9}$$

It should be noticed that the angle η_3 is associated with the local circular segment as shown in the diagram. The current position of the vehicle is specified by $r = R + d$ and θ. ψ indicates the velocity direction. η_2 is

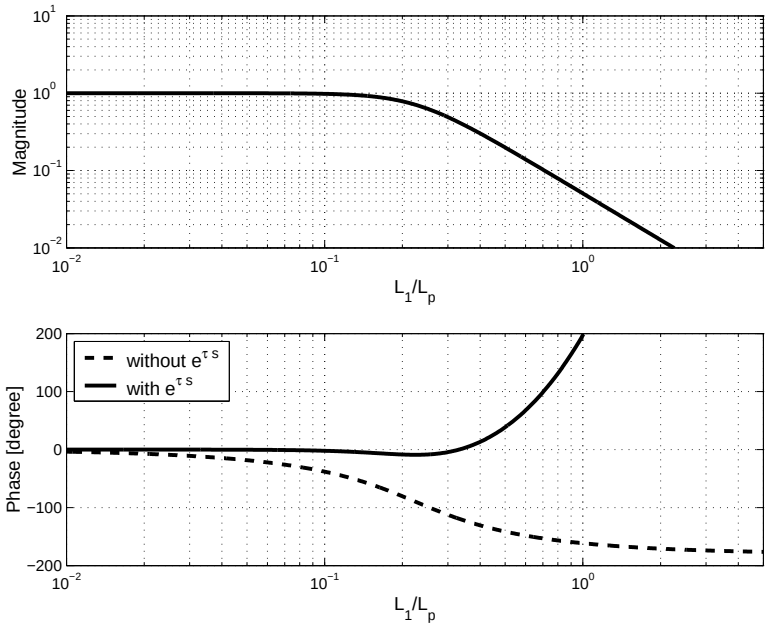

Figure 7. Frequency Response for Guidance Logic

an angle that is created by the difference between the velocity direction and the current tangent line to the circular desired path. The relation among the three angles is

$$\psi - \theta + \eta_2 = \frac{\pi}{2}$$

Then,

$$\dot{\psi} = \dot{\theta} - \dot{\eta_2} \tag{10}$$

Also, due to assumptions in Eq. (9) and using a similar relation in Eq. (2)

$$\sin \eta_3 \approx \frac{L_1}{2R} \tag{11}$$

We further define

$$c \equiv \cos \eta_3 \approx \sqrt{1 - \left(\frac{L_1}{2R}\right)^2} \tag{12}$$

Using the small angle assumption for η_2 the rate of change in position error is expressed as

$$\dot{d} = V \sin \eta_2 \approx V \eta_2$$

Therefore,

$$\ddot{d} \approx V \dot{\eta_2} \tag{13}$$

Also, using the relations in Eq. (10) and Eq. (13) the lateral acceleration is expressed as

$$a_{s_{cmd}} \approx V\dot{\psi} = V\dot{\theta} - V\dot{\eta_2} = V\dot{\theta} - \ddot{d}$$

With the small angle assumptions on η_1 and η_2

$$V\dot{\theta} \approx \frac{V^2}{R}$$

which is centripetal acceleration to follow the circle with radius R at speed V. Then

$$a_{s_{cmd}} \approx \frac{V^2}{R} - \ddot{d} \tag{14}$$

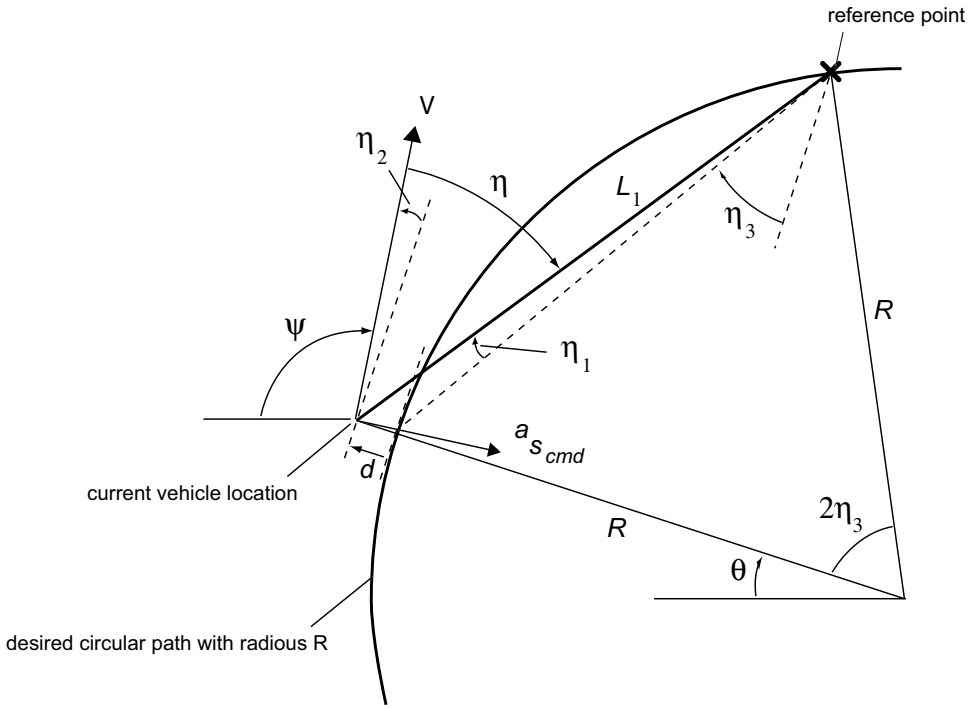

Figure 8. Circular Path Following Case

Using small angle assumptions for η_1 and η_2,

$$\begin{aligned} \frac{2V^2}{L_1}\sin\eta &= \frac{2V^2}{L_1}\sin\left(\eta_1+\eta_2+\eta_3\right) = \frac{2V^2}{L_1}\{\sin(\eta_1+\eta_2)\cos\eta_3+\cos(\eta_1+\eta_2)\sin\eta_3\} \\ &\approx \frac{2V^2}{L_1}\{\eta_1\cos\eta_3+\eta_2\cos\eta_3+\sin\eta_3\} \end{aligned} \tag{15}$$

With

$$\eta_1 \approx \frac{d}{L_1}\cos\eta_3, \qquad \eta_2 \approx \frac{\dot{d}}{V}$$

and applying Eq. (11) and Eq. (12), Eq. (15) reduces to

$$\frac{2V^2}{L_1}\sin\eta = \frac{2V^2c^2}{L_1^2}d + \frac{2Vc}{L_1}\dot{d} + \frac{V^2}{R} \tag{16}$$

Finally, substituting the relations in Eq. (14) and Eq. (16) to Eq. (1) yields

$$\ddot{d} + 2\zeta\omega_n\dot{d} + \omega_n^2 d \approx 0 \quad \text{where } \zeta = 0.707,\ \omega_n = \frac{\sqrt{2}Vc}{L_1} \tag{17}$$

Therefore $d \to 0$ as $t \to \infty$.

D. Comparison of the New Guidance Logic with the Traditional Linear Method

In the previous section, it was shown that the nonlinear guidance logic approximates a linear PD controller, on cross-track error, in following a straight line. This section will compare, by simulations, the performance of the nonlinear guidance logic and the associated linear controller, for various cases of trajectories and wind conditions.

In the simulation analysis presented below, 25 m/s of nominal vehicle speed and the separation distance(L_1) of 150 m were used for the associated linear controller given by Eq. (3).

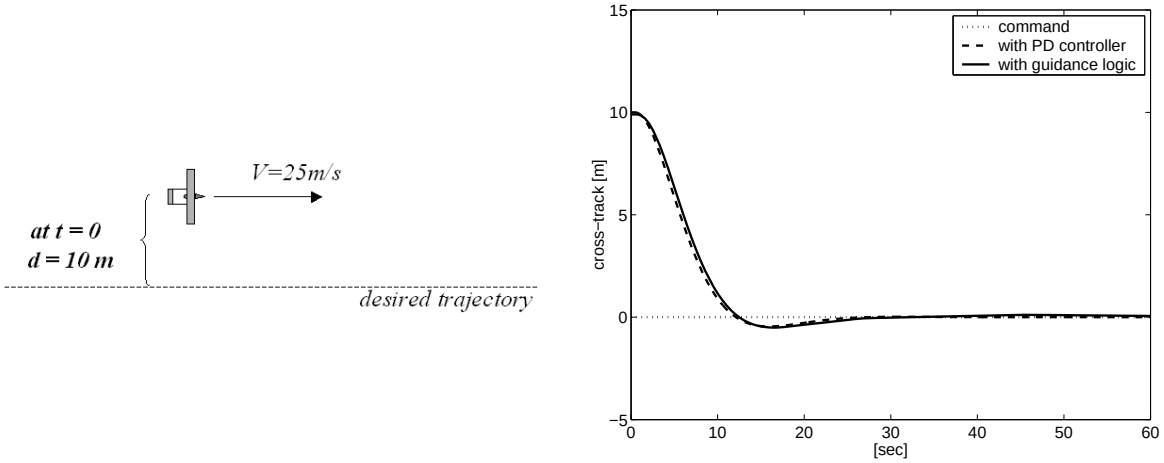

Figure 9. Comparison - Straight Line Following

Comparison 1 - Straight Trajectory Following

First, the two methods were applied for tracking a straight line. Figure 9 shows the simulation setup with an initial cross-track error of 10 meters and the associated results using the two methods. The simulation results indicate that the performances of the two methods are roughly the same in following a straight trajectory.

Comparison 2 - Curved Trajectory Following

Next, the two methods were applied to tracking a curved line. Figure 10 shows the simulation setup, the desired curved flight trajectory, and the associated simulation results. The aircraft is initially at level flight heading due north. The trajectory plot (a) in Figure 10 is the case where the linear controller was used. The PD controller resulted in a steady state error of about 40 meters. The steady state error can be explained by noting that the system is type 2. There are two pure integrators in the associated loop transmission with a plant model and the PD controller. The two integrators are from the kinematics of the plant model - from *acceleration input* to *position output*. The steady state error occurs because the position reference command for cross-track is imposed in a parabolic fashion, when the desired path is a circle.

In order to eliminate the steady state error, an integrator was added. The simulation result using the PID controller is now plotted on the same graph as a solid line. As can be seen the steady state error is removed by adding the integration controller. However, the error during the initial transition still remains.

On the other hand, the nonlinear guidance logic worked very well in following the curved path as indicated in Figure 10 (b). Deviation from the curved path was no more than 5 meters during the initial transient.

Comparison 3 - Curved Trajectory Following with Wind

Additional simulations were executed with similar conditions and with a five meter per second steady wind. The direction of the wind was from west to east. The vehicle initial condition and the wind condition are shown in Figure 11. The performance of the linear controllers (PD and PID) are shown in the trajectory plot (a) in Figure 11.

For the PD controller, the cross-track error varied in a range between 30 m and 60 m, after the initial transition period. For the PID controller, the cross-track error varied in the range between -20 m and +20 m after the initial transition period. A more careful look reveals that the vehicle flies outside the circular path when it is in the downwind region, and inside the circular path in the upwind region. The reason for this performance can be explained by noting that when the vehicle is in the downwind region, it moves faster with respect to an inertial frame. Under this condition, the vehicle must generate a larger acceleration command (or a larger bank angle command) if it is to follow the desired circular path. The linear feedback controller with fixed gain has an inherent limitation and cannot immediately remove the error, which is the result of inertial speed changes due to the wind.

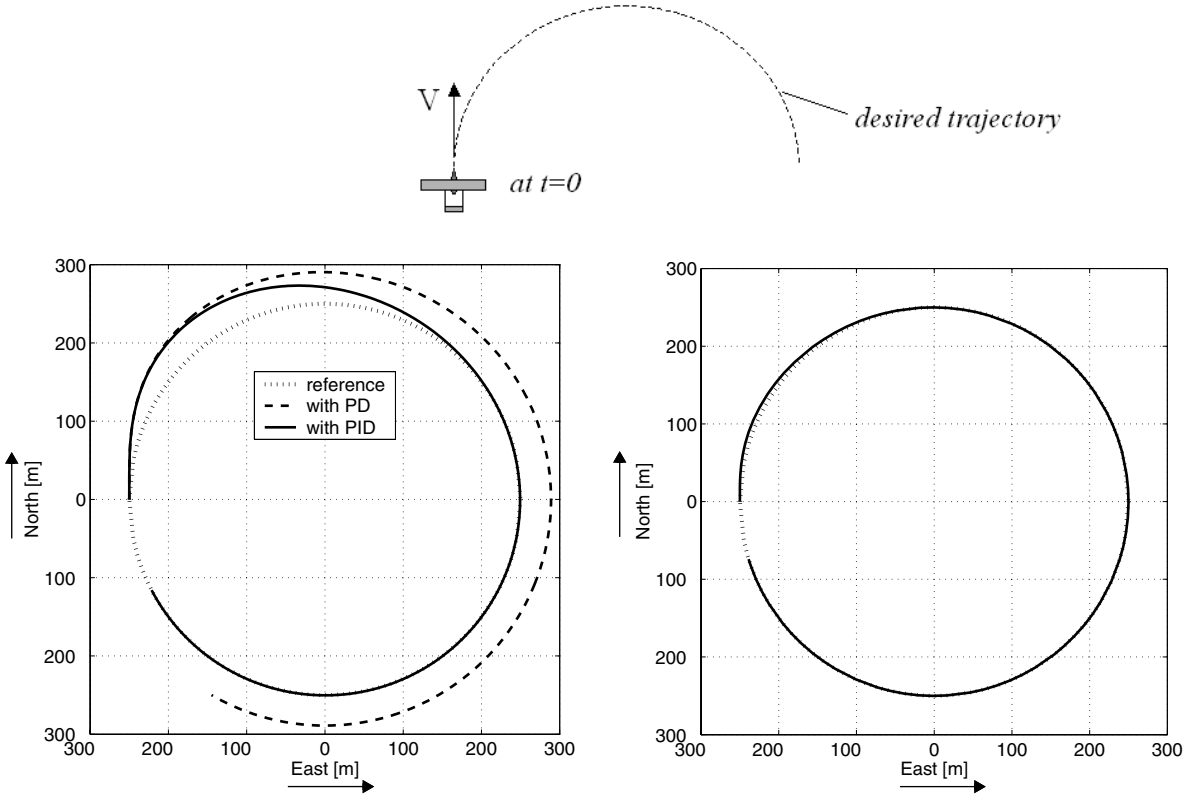

(a) PD, PID Linear Control (b) Nonlinear Guidance Logic

Figure 10. Comparison - Curved Line Following

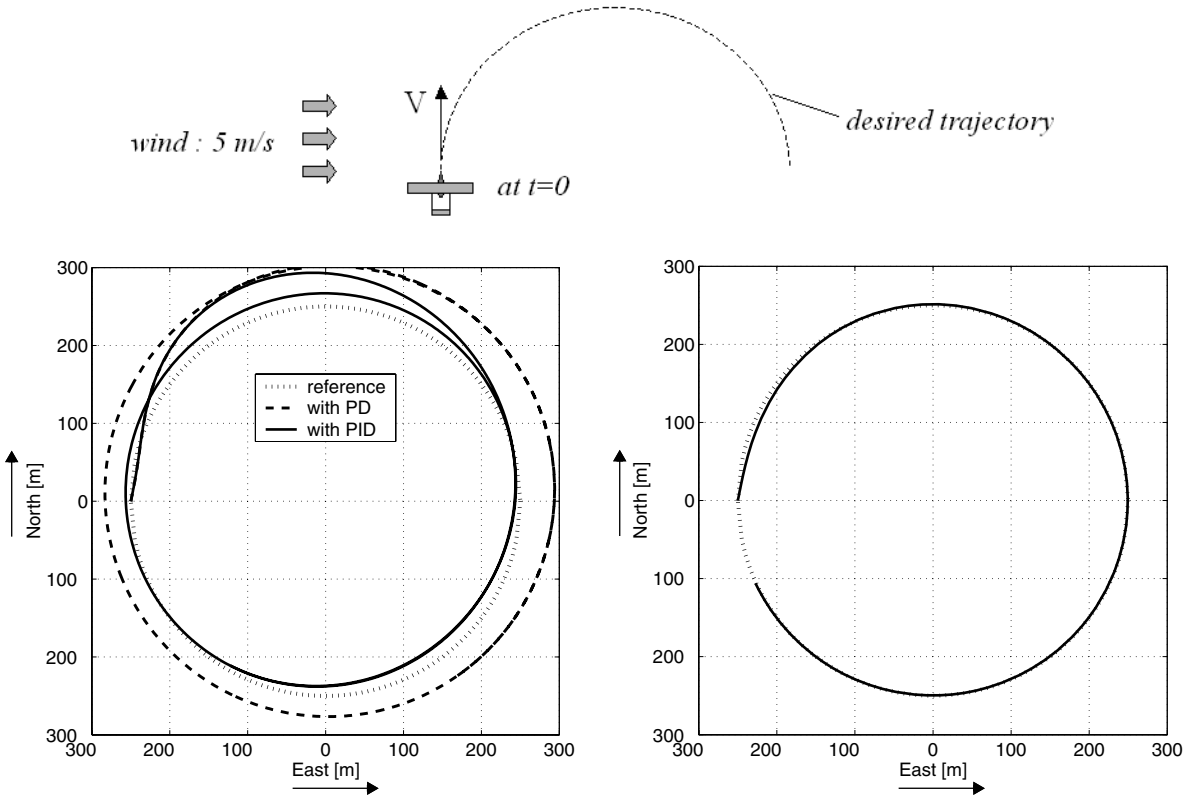

(a) PD, PID Linear Control (b) Nonlinear Guidance Logic

Figure 11. Comparison - Curved Line Following with Wind

(a) Mini Child Vehicle

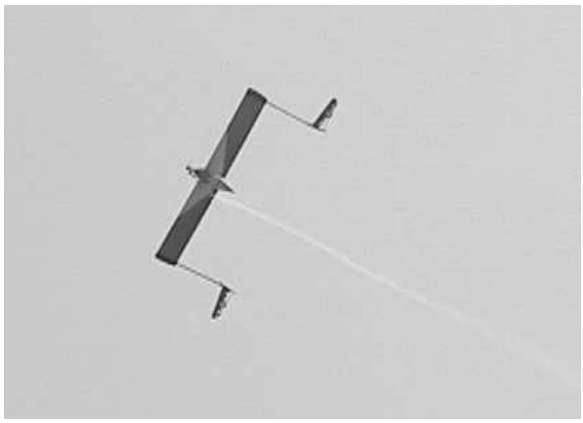

(b) OHS Parent Vehicle

Figure 12. Two UAVs in Parent Chicle Unmanned Air Vehicle Project

On the other hand, the nonlinear guidance logic method worked very well in following the curved path, in the presence of wind, as shown in Figure 11 (b) with errors less than 7 meters after the initial transient has decayed. The reason for the better performance in this case can be understood by the formula in Eq. (1)

$$a_{s_{cmd}} = 2\frac{V^2}{L_1}\sin\eta$$

where the vehicle ground speed (as a surrogate for inertial velocity) is used for V at each instant in generating the acceleration command. In other words, the nonlinear guidance logic takes into account the inertial velocity changes due to the wind effect, and adapts to the situation accordingly.

III. Flight Test

The guidance algorithm was implemented and tested with the two UAVs constructed in the Parent Child Unmanned Air Vehicle (PCUAV) project at MIT. In creating the required lateral acceleration, bank angle control was used in the inner loop. The associated outer-loop control bandwidth was limited by the inner-loop bank control bandwidth (2∼3 rad/s) and a GPS time delay of 0.4 seconds. Thus, with the nominal flight velocity of about 25 m/s, the choice of L_1=150 m results in the associated crossover frequency at 0.4 rad/s.

Figure 12 (a) shows the Mini Child vehicle. The vehicle has a wing span of 2.54 meters and its total weight, including onboard avionics, is 9.1 kilograms. Figure 12 (b) shows the Outboard Horizontal Stabilizer (OHS) configuration of the Parent vehicle. Aerodynamic and the associated stability features of this platform are found in Ref. [10, 11]. The vehicle has a wing span of 4.5 meters and its total weight is 20 kilograms.

Figure 13 shows the flight data for the Mini vehicle using the guidance logic for path following in the lateral direction. The plot shows the 2-dimensional trajectory of the Mini vehicle (solid line) with a commanded desired trajectory (dotted line). The small numbers along the trajectory are the flight times recorded in the onboard avionics. This plot indicates that the vehicle follows the commanded trajectory quite well. When the Mini vehicle flies along the circle the lateral displacement between the vehicle and the desired path remained within ±2 meters for the 75% of its flight time and within ±3 meters for 96% of the flight time.

A similar flight test was performed for the OHS Parent. Figure 14 shows the trajectory of the Parent vehicle and the commanded path. The autonomous control was activated at t=76 [sec] when the vehicle was near (-140 m E, 200 m N). The initial transient, during the flight time between 76 and 90 seconds, is due to the offset of the initial velocity vector. After the transient period, the trajectory of the vehicle followed the commanded path within ±2 meters for the 78% of its flight time and within ±3 meters for 97% of the flight time.

With the tight trajectory tracking capability of each aircraft it was demonstrated that the two vehicles can rendezvous from any arbitrary initial positions to a configuration of tight formation flight. The series of plots in Figures 15 show the positions of the Parent and the Mini in the north-east 2-D map. In the

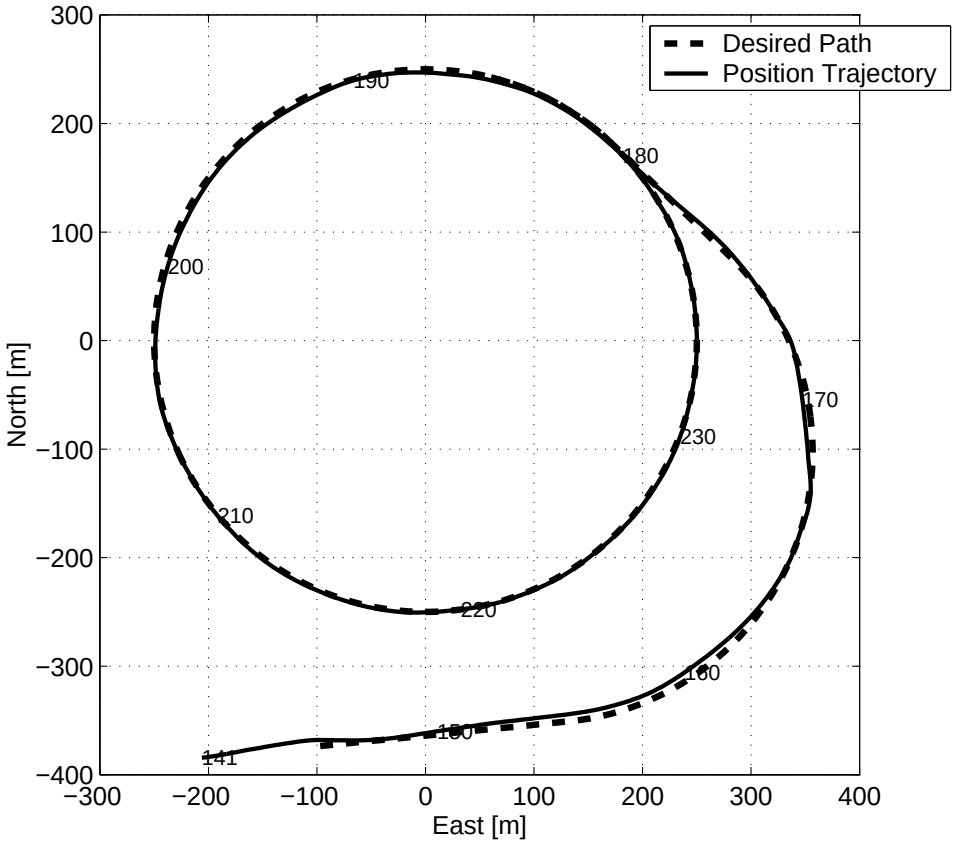

Figure 13. Flight Data of MINI - Trajectory Following

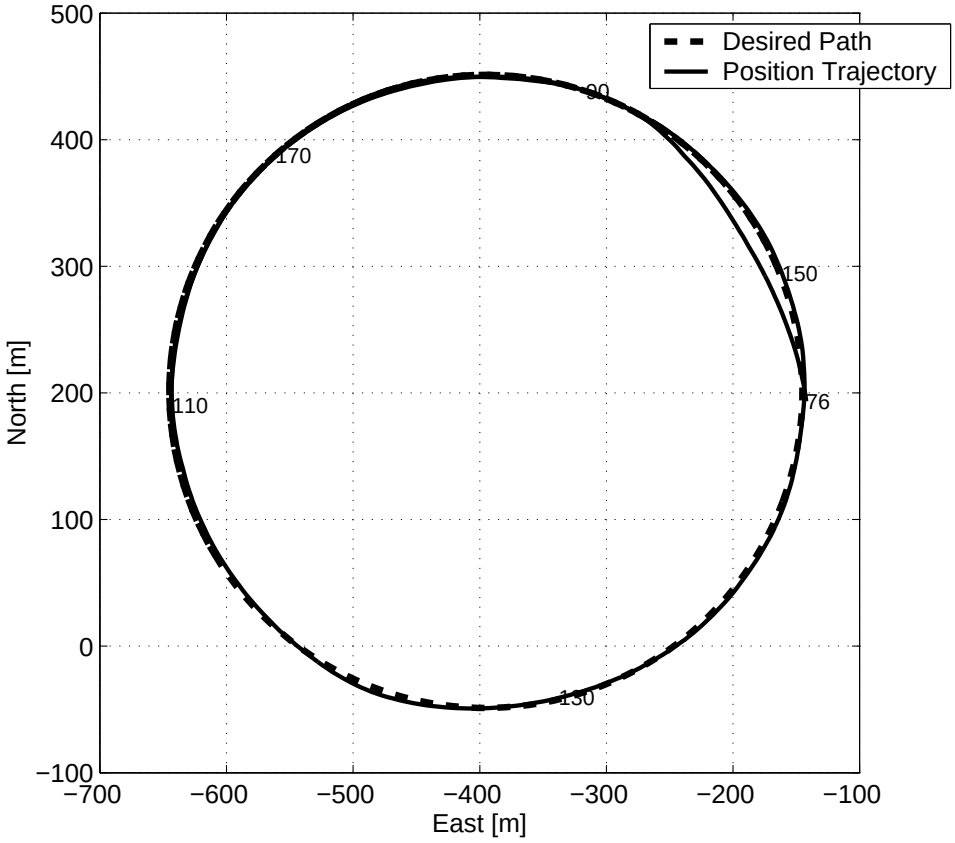

Figure 14. Flight Data of OHS Parent - Trajectory Following

test procedure, the OHS Parent vehicle follows the circular flight path, with no knowledge of the Mini vehicle's location. The Mini vehicle schedules its flight path and performs formation flight by receiving position information from the OHS Parent. The letter 'O' on each plot designates the location of the OHS

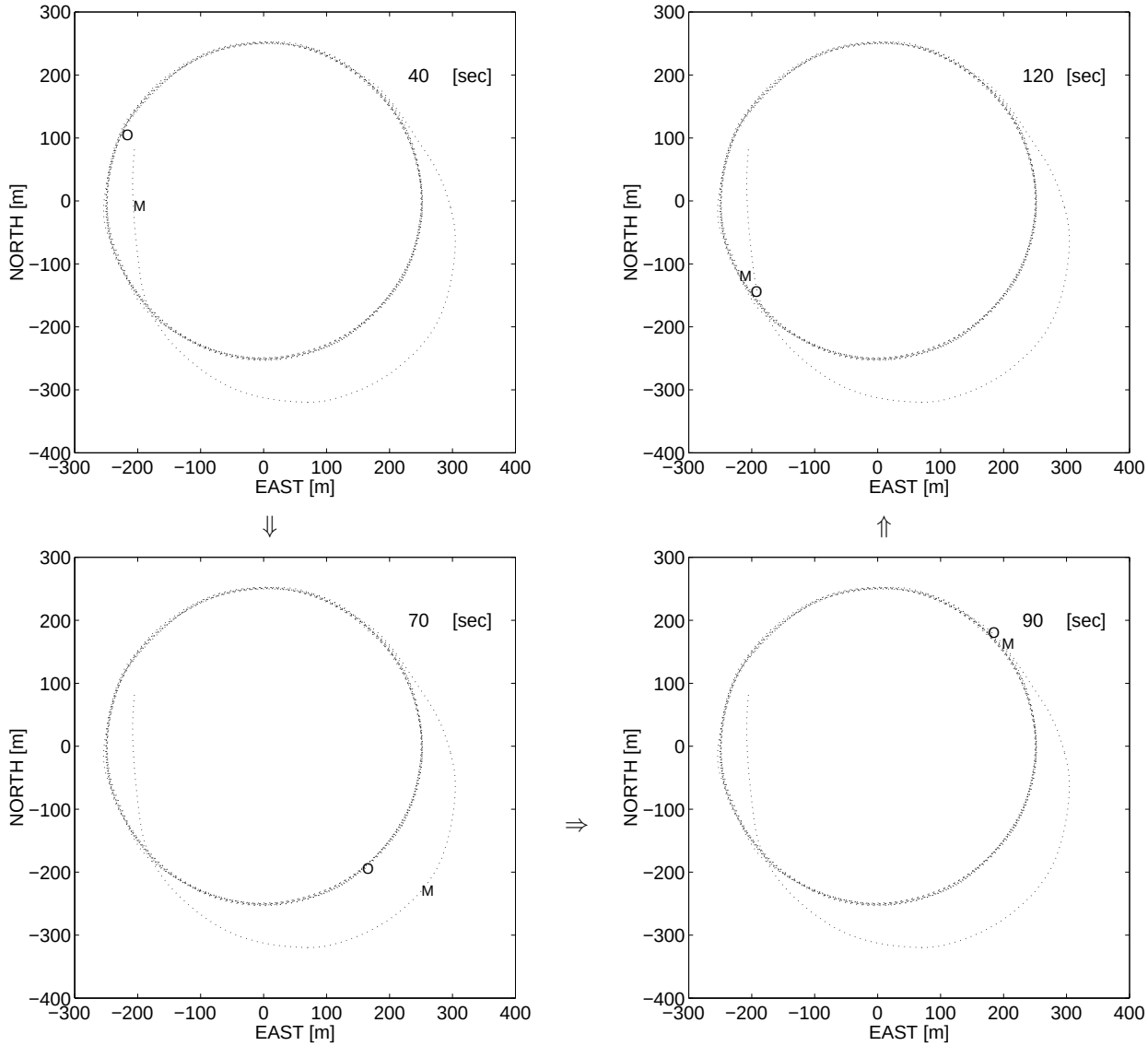

Figure 15. Flight Data - Rendezvous Trajectories of OHS and Mini (O:OHS, M:Mini)

Parent at each point in time, and 'M' designates the location of the Mini. The OHS Parent had been flying autonomously and maintaining a circular path when the Mini was switched to autonomous mode. The center of the circle is at the origin. The autonomous control of the Mini vehicle initiates at about 40 seconds when the Mini was near (-207 m E, -8 m N), and the Parent was at (-225 m E, 105 m N), and both UAVs were heading approximately south. From time=40 [sec] to 92 [sec], the Parent kept flying along the circle and the Mini generated and scheduled its path, and at about 92 [sec] the Mini entered the circle. From 92 [sec] onward the Mini was commanded to track the same circular path while maintaining the separation command relative to the Parent. Although the position plots presented here terminate at 120 [sec], the Mini and the Parent continued their flights making two and a half circuits of the circular path together before the Mini was switched back to the manual mode at 290 [sec].

Figure 16 shows a photo taken from the ground during the formation flight period. During formation flight the separation distance command was reduced gradually by a ground station command from an initial command of 30 meters, in steps, down to 12 meters. The first graph in Figure 17 shows the relative distance

Figure 16. Formation Flight during Flight Test (The Mini is commanded 12 meters behind and 2 meters above the Parent)

and the separation command. During the period of the entire formation flight from 92 seconds till 290

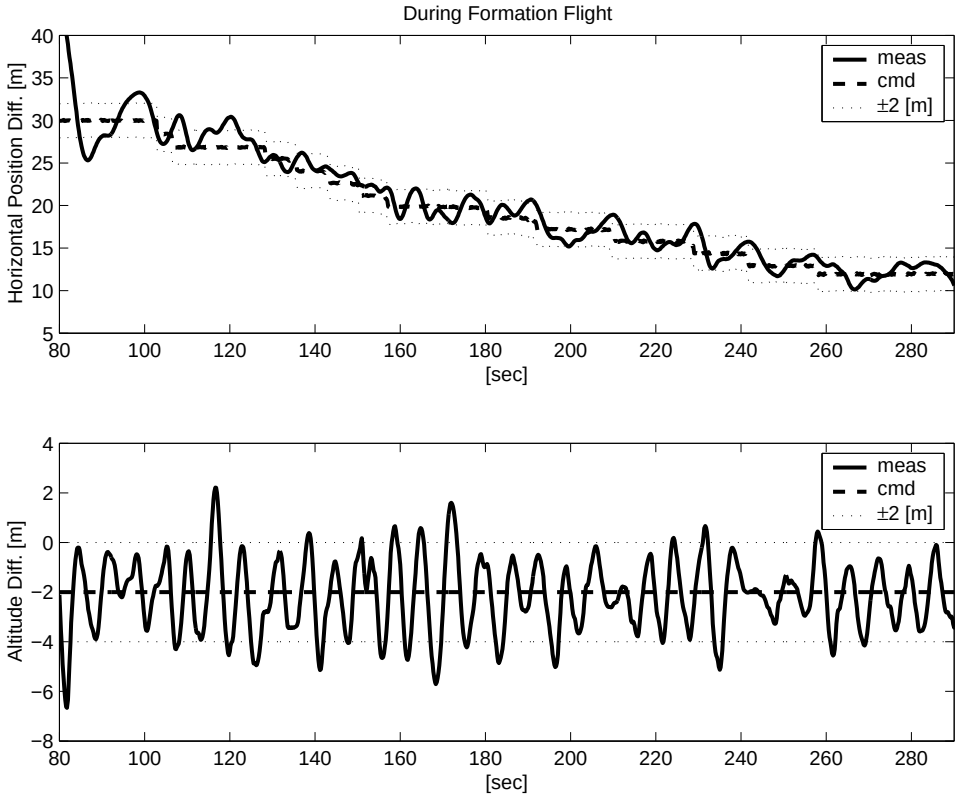

Figure 17. Flight Data of Relative Position Differences during Formation Flight

seconds the separation distance command was slowly reduced, and the Mini vehicle followed its command within an error of ±2 meters, for the 86% of this period.

The bottom graph in Figure 17 shows the altitude difference between the two vehicles during the formation flight. The command for the altitude difference was set to be 2 meters in this test, with Mini vehicle higher than OHS Parent. The altitude difference remained within ± 2 meters for 84% of the time. For longitudinal control, linear quadratic regulators were used for both vehicles [12].

IV. Conclusions

This paper discussed a new guidance logic for trajectory following and reported flight test results using this logic to control two UAVs. Using simulations, it was shown that with the new method a vehicle will follow a desired trajectory better than with the traditional linear technique. The reasons for the better performance can be explained as

1. The angle η used in the guidance logic serves three purposes. First, it provides a heading correction. Second, for small deviations from the desired trajectory it provides PD control on cross track error. And third, it provides an anticipatory acceleration command to exactly follow a circular reference trajectory.

2. The guidance logic uses the instantaneous vehicle inertial speed in the computation of the acceleration command. This kinematic factor adds an adaptive capability with respect to changes in vehicle inertial speed, due to external disturbances, such as wind.

Acknowledgments

The support by C.S.Draper Laboratory, Inc. is gratefully acknowledged.

References

[1]T. Keviczky and Gary J. Balas, "Software enabled flight control using receding horizon techniques," *AIAA Guidance, Navigation, and Control Conference and Exhibit*, (AIAA2003-5671), August 2003.

[2]R. M. Murray, "Trajectory generation for a towed cable system using differential flatness," *IFAC World Congress*, 1996.

[3]R. M. Murray and M. Rathinam, "Configuration flatness of Lagrangian systems underactuated by one control," *Control and Decision Conference*, 1996.

[4]E. Corban, E. Johnson, and A. Calise, "A six degree-of-freedom adaptive flight control architecture for trajectory following." *AIAA Guidance, Navigation, and Control Conference and Exhibit*, (AIAA-2002-4776), 2002.

[5]D.J. Yost J.E. Kain, "Command to line-of-sight guidance: A stochastic optimal contorl problem," *Journal of Spacecraft*, 14(7):438–444, 1977.

[6]P. Zarchan, *Tactical and Strategic Missile Guidance*, volume 176 of *Progress in Astronautics and Aeronautics*. AIAA, third edition, 1997.

[7]J. H. Blakelock, *Automatic Control of Aircraft and Missiles*. Wiley-Interscience, 1991.

[8]PCUAV web page, http://web.mit.edu/aeroastro/pcuav/, http://web.mit.edu/sanghyuk/www.

[9]S. Park, T. Jones, J. Deyst *et al.* "The parent and child unmanned aerial vehicle system," *Unmanned Vehicle Systems International Conference*, July 2003.

[10]J.A.C Kentfield, "Upwash flowfields at the tails and aircraft with outboard horizontal stabilizers." *Conference Paper, AIAA 98-0757*, Jan 1998.

[11]J. Mukherjee, *Automatic Control of an OHS Aircraft*, Ph.D. thesis, University of Calgary, 2000.

[12]S. Park. *Avionics and Control System Development for Mid-Air Rendezvous of Two Unmanned Aerial Vehicles*, Ph.D. thesis, MIT, February 2004.

Appendix

This section provides a nonlinear Lyapunov stability analysis for the case of following a straight line desired path. In Figure 18, the system model is expressed by the following set of the equations of motion

$$\dot{d} = V \sin \eta_2 \quad \text{and} \quad \dot{\eta_2} = -\frac{a_s}{V} \tag{18}$$

with the guidance logic

$$a_s = \frac{2V^2}{L_1} \sin \eta$$

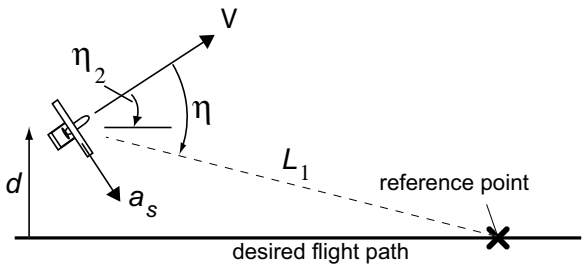

Figure 18. Model for Lyapunov Analysis for Straight Line Following Case

For the unique existence of the reference point we assume

$$d < L_1, \quad -\frac{\pi}{2} < \eta < \frac{\pi}{2} \tag{19}$$

Then

$$\mathcal{L} = \frac{1}{2}\left(V \sin\eta_2\right)^2 + \int_0^d \frac{2V^2}{L_1}\sin(\eta - \eta_2)dy \tag{20}$$

is a Lyapunov function. Since, from Figure 18,

$$\sin(\eta - \eta_2) = \frac{d}{L_1} \tag{21}$$

then Eq. (18) becomes

$$\mathcal{L} = \frac{1}{2}V^2 \sin^2\eta_2 + \frac{V^2}{L_1^2}d^2$$

which is a positive definite function. Next the time derivative of Eq. (20) is

$$\dot{\mathcal{L}} = V^2 \sin\eta_2 \cos\eta_2 \dot{\eta_2} + 2\frac{V^2}{L_1^2}d\dot{d}$$

Using Eq. (18) and Eq. (21) the expression for $\dot{\mathcal{L}}$ becomes

$$\dot{\mathcal{L}} = -\frac{2V^3}{L_1}\sin\eta_2\{\cos\eta_2 \sin\eta - \sin(\eta - \eta_2)\}$$

Finally, using

$$\sin(\eta - \eta_2) = \sin\eta\cos\eta_2 - \cos\eta\sin\eta_2$$

$\dot{\mathcal{L}}$ is reduced to

$$\dot{\mathcal{L}} = -\frac{2V^3}{L_1}\sin^2\eta_2\cos\eta \tag{22}$$

which is negative semi-definite since $|\eta| < \pi/2$ from Eq. (18). Then, applying the invariant set theorem, the set defined by $\dot{\mathcal{L}} = 0$ contains no trajectory other than $(\eta_2 = 0,\ d = 0)$. Therefore, $(\eta_2 = 0,\ d = 0)$ is asymptotically stable for $d < L_1$, $|\eta| < \pi/2$